Small-scale temperature fluctuations associated with gravity waves cause additional radiative cooling of mesopause the region

Alexander A. Kutepov,[1,2,3] Artem G. Feofilov,[3,4] Alexander S. Medvedev,[5] Adalbert W. A. Pauldrach,[1] and Paul Hartogh[5]

Received 23 October 2007; accepted 9 November 2007; published 22 December 2007.

[1] We present a study of the radiative cooling of the mesosphere and lower thermosphere in the infrared bands of CO_2, O_3 and H_2O due to small-scale irregular temperature fluctuations caused by gravity waves. These persistent fluctuations are presently not well represented by general circulation models. A statistical model of gravity wave-induced temperature variations was applied to large-scale temperature profiles, and the corresponding direct radiative calculations were performed. We show that temperature fluctuations can cause an additional cooling up to 3 K day^{-1} near the mesopause. The effect is produced mainly by the fundamental 15 μm band of the main CO_2 isotope. We found a simple correction depending on the temperature fluctuations variance, which should be added in radiative calculations to the mean temperature profile to account for the additional cooling associated with the unresolved disturbances. **Citation:** Kutepov, A. A., A. G. Feofilov, A. S. Medvedev, A. W. A. Pauldrach, and P. Hartogh (2007), Small-scale temperature fluctuations associated with gravity waves cause additional radiative cooling of mesopause the region, *Geophys. Res. Lett.*, *34*, L24807, doi:10.1029/2007GL032392.

1. Introduction

[2] Numerous observations of instantaneous vertical temperature profiles in the middle atmosphere show a highly irregular small-scale structure associated with gravity waves (GW) and/or turbulence [*Fritts and Alexander*, 2003, and references therein]. The amplitudes of these variations are usually in the range of several degrees and increase with height. Occasionally they can exceed tens of degrees during passages of strong GW packets. In the lower thermosphere, the magnitude of fluctuations ceases its growth due to the filtering and absorption of waves. Since these waves are not well resolved by contemporary general circulation models (GCMs), their effects are usually accounted for in middle atmosphere GCMs in the form of so-called "GW drag" schemes (see *Fritts and Alexander* [2003] for references) and the associated dynamically induced heating/cooling rates [e.g., *Medvedev and Klaassen*, 2003].

[3] Radiative cooling strongly depends on the background atmospheric temperature and, therefore, must be affected by the irregular temperature fluctuations (ITF) associated with GW, especially in the mesosphere and lower thermosphere (MLT). However, due to the breakdown of the local thermodynamic equilibrium (non-LTE), radiative calculations in the MLT become increasingly complicated and computationally expensive. As a result, various parameterizations for non-LTE radiative cooling/heating rates are employed in the models, see, for instance, the parameterizations of *Zhu* [1989], *Kutepov and Fomichev* [1993] and *Fomichev et al.* [1993] for the CO_2 cooling. Besides various simplifications, which reduce the accuracy, these parameterizations normally calculate heating rates on vertical grids even sparser than the model resolution, followed by the interpolation onto the model grids. Only recently a code was developed which computes accurate non-LTE radiative cooling/heating fast enough to be used on GCM grids as a replacement for these parameterizations [*Hartogh et al.*, 2005]. However, neither the exact algorithm nor parameterizations can account for the influence of unresolved small-scale ITFs. Moreover, to our knowledge, no studies have been performed to estimate the influence of subgrid-scale ITFs on the radiative cooling/heating in the atmosphere.

[4] In this paper we estimate the effect of ITFs on the infrared radiative cooling in the MLT. Section 2 describes a model for the GW induced temperature fluctuations. Radiative calculations in the MLT are outlined in section 3. Section 4 discusses the calculation approach as well as the results, interpretation and parameterization of obtained effects for CO_2. Section 5 describes the influence of ITFs on the O_3 and H_2O cooling. The Conclusion summarises results and provides recommendations for implementations in GCMs.

2. Stochastic Model of Gravity Waves

[5] Temperature variations associated with GW are highly complex and irregular. In many observational studies their properties are usually summarized in the form of averaged spectra. Here we applied a simplified model described below which randomly generates individual temperature profiles reminiscent of instantaneous measurements during periods of strong GW activity, whose statistical properties agree with observed GW spectra. Since individual profiles cannot be reconstructed from observed spectra, the model required additional plausible assumptions.

[1]University Observatory Munich, Faculty for Physics, Ludwig Maximilian University, Munich, Germany.
[2]Department of Physics, Catholic University of America, Washington, D. C., USA.
[3]NASA Goddard Space Flight Center, Greenbelt, Maryland, USA.
[4]Oak Ridge Associated Universities, Oak Ridge, Tennessee, USA.
[5]Max Planck Institute for Solar System Research, Katlenburg-Lindau, Germany.

0094-8276/07/2007GL032392

[6] A vertical temperature distribution created by GW can be represented as a sum of individual harmonics:

$$T'(z) = \sum_k T_k(z) = \sum_k \hat{T}_k(z_0) \exp\left(i \int_{z_0}^{z} m_k(z')dz' + \phi_k\right), \quad (1)$$

where $\hat{T}_k(z_0)$ is the amplitude of the k-th harmonic at the source level z_0, $m_k(z) = m_k^{(R)} + im_k^{(I)}$ is its complex vertical wavenumber, ϕ_k is the phase. This yields for each k

$$dT_k/dz = im_k T_k. \quad (2)$$

If $T_k(z_0)$, $m_k(z_0)$, and ϕ_k are known at the source level, (2) can be integrated vertically for each harmonic k to obtain the profile $T'(z)$. Real parts of the vertical wavenumbers $m_k^{(R)}$ for GW harmonics are, generally, functions of z as they depend on the refractive properties of the atmosphere determined by the background wind and temperature. However, $T_k(z)$ is not an individual plane wave, but rather a sum of GW harmonics with different phase velocities travelling at different angles to the mean wind. Here we assume no vertical dependence for $m_k^{(R)}$ since there exists no rigorous requirement for the opposite in the given formulation. This also helps to make the calculations tractable. The imaginary part of the vertical wavenumber, $m_k^{(I)}$, should include the effects of the amplification due to the air density decrease, damping by the molecular viscosity, and the effect of amplitude saturation which limits the instantaneous temperature gradients by the value of the adiabatic lapse rate, i.e., $\bar{T}_z + T'_z \geq -gc_p^{-1}$, c_p being the specific heat capacity, g is the acceleration of gravity. The first two effects enter (2) in the form [see, e.g., *Vadas and Fritts*, 2005]

$$m_k^{(I)} = -1/2H(z) + \mu m_k^{(R)3}/(\rho\omega), \quad (3)$$

where H is the scale height; $\mu = 0.017$ gm^{-1}s^{-1} is the molecular viscosity, ρ is the density, and ω is the assumed frequency of the harmonic. In our calculations, ω served as a tuning parameter to ensure that all wave disturbances dissipate above the turbopause. A "convective adjustment scheme" turns on to modify the temperature $T'(z)$ when the net vertical gradient of the potential temperature becomes negative.

[7] We use the canonical "modified DeSaubies" vertical wavenumber spectrum to prescribe the wave field at the source level $z_0 = 15$ km: $S(m/m_*) = A_0(m/m_*)^s[(1 + (m/m_*)^{s+3}]^{-1}$, where S is the wave spectral density, and the values for the following parameters were borrowed from *Medvedev and Klaassen* [2000]: $s = 0$ or 1, $m_* = 0.006$ m^{-1}, $A_0 = 10$ to 100. The algorithm of the temperature profile generation is as follows. First, several vertical wavenumbers $2\pi\lambda_{\max}^{-1} \leq m_k^{(R)} \leq 2\pi\lambda_{\min}^{-1}$ and the corresponding phases ϕ_k are randomly generated, where $\lambda_{\max}$ and $\lambda_{\min}$ are the longest and shortest vertical wavelengths, respectively. The amplitudes of the harmonics are assigned according to the DeSaubies spectrum. Then, (2) is integrated upward to produce an individual profile $T'(z)$. There is ample evidence [e.g., *Fritts and Alexander*, 2003, section 4.3] that GW spectra in the atmosphere are composed of only a few harmonics rather than represent a broad mix of waves. *Sica and Russell* [1999] argued that, in observations, the spectra most often are dominated by 1 to 3 waves. We use 2 GW harmonics in our simulations.

[8] The following parameters have been used in the calculations presented below: the vertical grid step $\Delta z = 300$ m, $A_0 = 40$, $s = 0$, $\lambda_{\max} = 11$ km, $\lambda_{\min} = 2.5$ km. As there is no data on the frequency of occurrence of waves with different vertical wavenumbers in observations, we assumed the same probability for harmonics with all wavelengths.

3. Infrared Radiative Cooling of MLT

[9] The radiative cooling of the MLT is affected mainly by the vibration-rotational bands of CO_2 around 15 μm. Effect of the 9.6 μm O_3 band is next in importance and contributes up to 25% of the total cooling at and around the stratopause. The water vapor cooling (dominated by the H_2O rotational band) plays a tertiary role contributing about 5–7% of the total IR cooling of the MLT.

[10] The radiative cooling/heating of the atmosphere h is described by the radiative flux divergence taken with the minus sign. Integrating the radiative transfer equation over the total solid angle Ω and frequency ν, one obtains

$$h = -\int d\Omega \int d\nu \frac{dI_{\Omega\nu}}{ds} = \chi(J - S), \quad (4)$$

where $I_{\Omega\nu}$ is the radiative intensity, $J = (1/4\pi\chi) \int d\Omega \int d\nu \chi(\nu) I_{\Omega\nu}$ is the mean radiative intensity, $S = \eta(\nu)/\chi(\nu)$ is the source function defined as a ratio of the atmospheric emissivity $\eta(\nu)$ and opacity $\chi(\nu)$, and $\chi = \int \chi(\nu)d\nu$ is the mean atmospheric opacity in the spectral region under consideration. χS in (4) describes the radiative loss of energy by a unit volume, and χJ describes the absorption by the same unit volume of the radiation coming from other atmospheric layers, the upwelling radiation from the surface, and the solar radiation.

[11] In the lower atmosphere, inelastic molecular collisions determine the population of molecular levels. As a result local thermodynamic equilibrium (LTE) exists, where the populations n_v of molecular vibrational levels v obey the Boltzmann law with the local kinetic temperature T_{kin}, and S in (4) is equal to the Planck function $B_\nu(T_{kin})$. In the middle and upper atmosphere, the frequency of collisions is low, and other processes which populate and depopulate molecular levels (such as an absorption and emission of the radiation in molecular bands, redistribution of excitation between colliding molecules, chemical excitation, etc.) must be taken into account. Under these non-LTE conditions n_v deviate from the Boltzmann distribution for the local T_{kin}, and S is no longer equal to $B_\nu(T_{kin})$. Non-LTE n_v are found from a set of rate equations expressing a balance of all processes, which populate and depopulate vibrational levels v, and the radiative transfer equation in the vibration-rotational bands.

4. Effect of ITFs on the CO_2 Cooling

[12] The bands of four CO_2 isotopes $^{12}C^{16}O_2$[0.984], $^{13}C^{16}O_2$[1.1×10^{-2}], $^{16}O^{12}C^{18}O$[3.9×10^{-3}] and $^{16}O^{12}C^{17}O$[7.3×10^{-4}] (hereafter denoted as 626, 636, 628

and 627, respectively), where the numbers in the brackets give the isotopic abundances, contribute to the thermal radiative cooling/heating of the MLT [*López-Puertas and Taylor*, 2001]. Among them the 15 μm fundamental band (FB) of the isotope 626 is the main contributor. Next in importance are the collective effect of the 15 μm FBs of the isotopes 636, 628 and 627, and that of the first hot (FH) and second hot (SH) bands of the isotope 626. For all these bands LTE breaks down above approximately 70–75 km for both day and night time conditions.

4.1. Calculation Procedure and Inputs

[13] We applied the ALI-ARMS (Accelerated Lambda Iteration for Atmospheric Radiation and Molecular Spectra) code [*Kutepov et al.*, 1998; *Gusev and Kutepov*, 2003] for solving the non-LTE problem in the CO_2 and calculating the radiative cooling/heating. 60 vibrational levels and 150 vibrational-rotational bands of four CO_2 isotopes were taken into account. They included a large number of weak combinational bands that absorb the near-infrared solar radiation during day time. The set of collisionally induced vibrational-translational (V-T) and vibrational-vibrational (V-V) energy exchange processes and the rate coefficients correspond to those described by *Shved et al.* [1998].

[14] We examined five atmospheric models corresponding to the summer solstice in the Northern hemisphere: at $-70.0°$ for the subarctic winter (SAW), $-40.0°$ for the midlatitude winter (MLW), $0.0°$ for the tropics (TROP), $40.0°$ for the midlatitude summer (MLS), and $70.0°$ for the subarctic summer (SAS). The local noons were set for each model with the Solar zenith angles of 93.5°, 63.5°, 23.5°, 16.5°, and 46.5°, respectively. T, p, $[N_2]$, $[O_2]$ and $[O(^3P)]$ were taken from the MSISE-90 model, the volume mixing ratio profiles of CO_2 correspond to the mean profile retrieved in the CRISTA experiments (C_C) and to that from earlier rocket-borne mass spectrometer experiments (C_R) [*Kaufmann et al.*, 2002]. $C_C(z)$ deviates from well mixed values between 70 and 80 km and is significantly lower above these altitudes than $C_R(z)$, which remains constant up to 90 km.

[15] For each temperature model $T(z)$, 1000 individual ITF profiles $T'(z)$ were randomly generated as described in Section 2. The non-LTE problem was solved and $h(z)$ computed for each profile $T(z) + T'(z)$, as outlined in Section 3. The mean $\overline{h(z)}$ was then obtained by averaging $h(z)$ at each altitude z. It was compared with the cooling $h_T(z)$ for the mean temperature profile $T(z)$.

4.2. Results of Calculations

[16] Figure 1 illustrates the calculations for the MLW model and $C_C(z)$. The variance profile (Figure 1a) $\sigma_T(z) = \{\overline{[T'(z)]^2}\}^{1/2}$ computed from all 1000 distributions of $T'(z)$ agrees reasonably well with observations (e.g., *Whiteway and Carswell* [1995], albeit in the Northern Hemisphere). Other panels show the mean profile $T(z)$ with σ_T superimposed (Figure 1b), $h_T(z)$ for the mean $T(z)$, $\overline{h(z)}$, with the respective variance σ_h (Figure 1c), and $\Delta h(z) = \overline{h(z)} - h_T(z)$ (black line) (Figure 1d).

[17] In Figure 2, profiles $T(z)$ (Figure 2a), $h_T(z)$ and $\overline{h(z)}$ (Figure 2b), and $\Delta h(z) = \overline{h(z)} - h_T(z)$ (Figure 2c) are shown for five selected temperature models for $C_C(z)$. It is seen that for SAW, MLW and TROP, both $h_T(z)$ and $\overline{h(z)}$ remain negative for almost all altitudes (with the exception of the weak heating for TROP in a narrow altitude region around 70 km). For MLS and SAS with their low mesospheric temperatures, appreciable heating due to the absorption of the upwelling radiation from the warmer lower atmosphere and Solar radiation is observed at 75–93 km (up to 3.3 K/day). It is seen in Figure 2c that the superimposed ITFs produce an additional cooling at 70–120 km for all the temperature models. This difference is greater for the profiles $T(z)$ that provide higher net cooling rates (compare SAW, MLW and TROP with MLS and SAS). For MLW, this additional cooling reaches 2.2 K/day at 94 km, however, it quickly vanishes outside the altitude region with strong ITF amplitudes. For $C_R(z)$ the additional cooling is observed at the same heights, it is about 1.4–1.8 times higher than that for $C_C(z)$ reaching the maximum value of 3.0 K day^{-1} for MLW at 94 km.

[18] A more detailed examination of the additional cooling induced by ITFs for MLW is presented in Figure 1d for $C_C(z)$. The effect is caused mainly by the 15 μm 626 FB transition (compare black and red lines). It is significant near the mesopause where it exceeds for this model the collective warming effect of the weak CO_2 hot and isotopic bands (compare the black line with the orange one showing the warming effect of weak bands $h_T(z) - h_{T,626FB}(z)$, where $h_{T,626FB}(z)$ is the radiative cooling/heating for the 15 μm 626 FB transition).

4.3. Interpretation and Parameterization

[19] The equation for the source function in the 626 FB, which provides the main contribution to both net and additional ITF-induced cooling, can approximately be presented in the MLT [*Kutepov and Fomichev*, 1993] both at day and night as a two-level problem

$$S = \lambda J[S] + (1 - \lambda)B. \tag{5}$$

In (5), $S \propto n_1/n_0$; n_1 and n_0 are the populations of the first excited vibrational level and the ground level, respectively; $\lambda = A/(A + C)$ is the probability of the photon to be re-emitted in the band after the act of absorption, A and C are the Einstein coefficient for the spontaneous emission in the band and the total collisional quenching rate of the upper vibrational level, respectively; $J[S] = \int K(z, z')S(z')dz'$ is the mean radiative intensity in the band in the integral form following from the formal solution of the radiative transfer equation, and B is the Planck function for the band center frequency ν_0. Since the overlapping of various bands is weak at considered altitudes, (4) is valid also for a single 626 FB. Then it follows from (4) and (5) that

$$h_{T,626FB}(z) = \chi(1 - \lambda)(J[S] - B). \tag{6}$$

Taking into account relatively weak temperature dependences of the collisional quenching rate C, mean opacity χ and transmittance derivatives $K(z, z')$, averaging (6) over all ITFs, and denoting thus averaged quantities with overbars, one derives, that $\overline{h_{T,626FB}}$ can be estimated by applying in (6) the mean source function $\overline{S}$ and Planck function $\overline{B}$. On the other hand, averaging (5) one obtains that $\overline{S}$ satisfies this equation with the Planck function B replaced by $\overline{B}$. It means that $\overline{h_{T,626FB}}$ can be estimated from a single application of the non-LTE radiation code to (5) with the temperature profile $\widetilde{T}(z)$ obtained from the relation

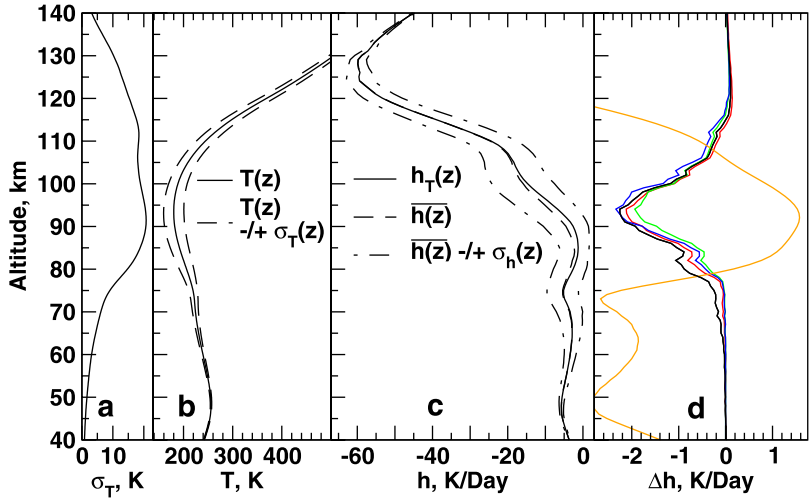

Figure 1. Effect of the small-scale irregular temperature fluctuations (ITFs) caused by gravity waves on the radiative cooling in the infrared bands of CO_2, midlatitude winter, CRISTA mean CO_2 VMR. (a) $\sigma_T(z)$; (b) $T(z)$ and $T(z) \mp \sigma_T(z)$; (c) $h_T(z)$, $\overline{h(z)}$ and $\overline{h(z)} \mp \sigma_h(z)$; (d) $\Delta h(z) = \overline{h(z)} - h_T(z)$ (black), $\Delta h_{626FB}(z) = \overline{h_{626FB}(z)} - h_{T,626FB}(z)$ (red), simulation of $\Delta h(z)$ by applying (7) with $\nu_0 = 667.4$ cm^{-1} (green) and $\nu_0 = 750.0$ cm^{-1} (blue), $h_T(z) - h_{T,626FB}(z)$ (orange).

$\overline{B[T(z) + T'(z)]} = B[\widetilde{T}(z)]$. Using the smallness of $T'(z) \ll T(z)$ to expand $B(T + T')$ into the Taylor series and averaging over all T', we obtain that $\widetilde{T}(z)$ can be represented as $\widetilde{T}(z) = T(z) + \Delta T(z)$ with

$$\Delta T(z) = \frac{1.44\nu_0}{2T^2(z)}\left[1 - \frac{2T(z)}{1.44\nu_0}\right]\overline{[T'(z)]^2}. \quad (7)$$

Note that the linear term in $T'(z)$ vanishes in this expression under averaging.

[20] Equation (6) explains why the ITFs cause an additional cooling between 70 and 120 km. There, the positive $\Delta T(z)$ directly increases the local cooling term associated with $-\overline{B}$. On the other hand, the non-local integral heating term J is less sensitive to the increase of the local temperature because of the contribution of the upward radiation fluxes, which are less affected by the ITFs in the lower atmosphere.

[21] We tested the parameterized temperature correction (7) for 5 atmospheric models and found that $h_{\widetilde{T}}(z)$ reproduces well $\overline{h(z)}$. Figure 1d demonstrates this for MLW. The green line corresponds to $\Delta h(z)$ for $\Delta T(z)$ from (7) with $\nu_0 = 667.4$ cm^{-1} of the 626 FB. Considering ν_0 as a free parameter we found that a better agreement for all the models is reached by applying $\nu_0 = 750.0$ cm^{-1} (blue line).

[22] Above ≈80 km, the O(^{3}P) atoms start dominating the quenching of the CO_2 ν_2 vibrations [*López-Puertas and Taylor*, 2001]. As a result the CO_2 radiative cooling in this region strongly depends on the product [O(^{3}P)] × K_O, which provides the atomic oxygen contribution to the total quenching rate C. h and Δh discussed above were obtained for the high value of quenching rate coefficient $K_O = 6 \times 10^{-12}$ cm^3 s^{-1} (for T = 300°K), retrieved from the space observations of 15 μm emissions [*Sharma and Wintersteiner*,

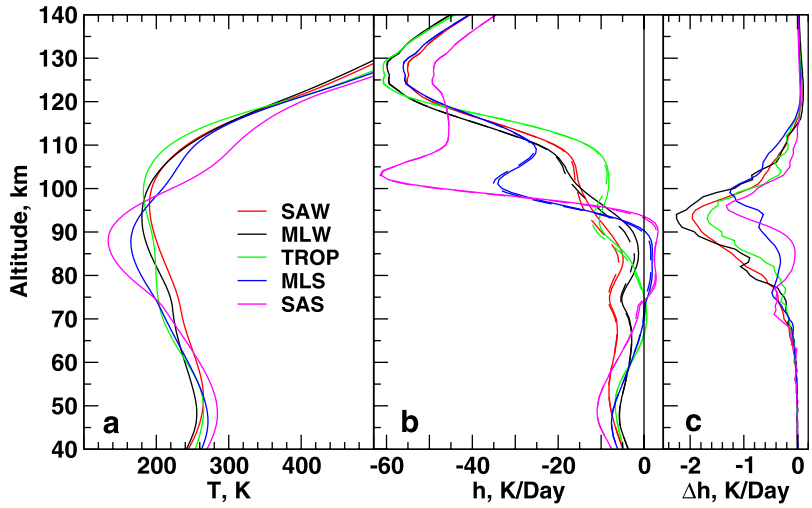

Figure 2. (a) Selected temperature profiles used in the calculations, (b) corresponding estimates of $h_T(z)$ (solid) and $\overline{h(z)}$ (dashed), and (c) $\Delta h(z) = \overline{h(z)} - h_T(z)$.

1990]. Application of the lower $K_O = 1.5 \times 10^{-12}$ cm^3 s^{-1}, which is more consistent with its recent laboratory measurements [*Castle et al.*, 2006], reduces the maximum value of the additional cooling caused by the ITFs to about 1 K/day for $C_C(z)$ and 1.4 K/day for $C_R(z)$, following the drop of the ratio $1 - \lambda = C/(C + A)$ in (6).

5. Effects of ITFs on the O_3 and H_2O Cooling

[23] Following the calculation procedure described in sub-section 4.1 we applied the ALI-ARMS code for 5 selected atmospheric models to estimate the effect of ITFs on the cooling of the MLT in the O_3 9.6 μm and the H_2O rotational bands. [O_3] for these calculations were taken from the SABER current V1.07 data product. [H_2O] were those from the HALOE current V19 data product. The H_2O rotational band is in LTE throughout the MLT, whereas the O_3 9.6 μm band departs from LTE above the altitude of 65–70 km. We utilized the model of non-LTE in O_3 developed by *Manuilova et al.* [1998]. It was found that the O_3 9.6 μm additional cooling caused by ITFs reached between 90 and 100 km 0.3, 0.24, 0.15, 0.1 and 0.05 K day^{-1} for the SAW, MLW, TROP, MLS, and SAS models, respectively. The same effect for the H_2O rotational band did not exceed 0.05 K/day for all the models considered. We also found that the additional cooling can be well accounted for by correcting the input temperature by means of (7) with $\nu_0 = 1043$ and 500 cm^{-1} for O_3 and H_2O, respectively.

6. Conclusions

[24] We performed a numerical investigation of the effect of small scale irregular temperature fluctuations (ITFs) associated with gravity waves, which are presently not captured by GCMs, on the radiative cooling of the mesosphere and lower thermosphere (MLT) in the CO_2, O_3 and H_2O infrared bands. We found that ITFs affect the radiative transfer and cause an additional cooling. In the periods of strong wave activity it can reach the maximum value of 2.5–3.3 K day^{-1} for a midlatitude winter mesopause region, where it exceeds the collective warming effect of the weak hot and isotopic CO_2 bands. The effect is produced mainly by the fundamental 15 μm band of the CO_2 isotope. We explained it by the increased mean local thermal emission compared to that for the non-disturbed temperature due to the strong non-linear temperature dependence of the Planck function. We found a simple expression for the correction to the input temperature profile to account for the additional cooling effect. As follows from (7), this correction ΔT depends on the mean variance of the perturbations, $\overline{[T'(z)]^2}$. For applications in GCM, this quantity can be obtained from GW parameterizations which normally calculate the wind variance for GW fluctuations, $\overline{[u(z)']^2}$. The variance $\overline{[T'(z)]^2}$ can readily be computed from the variance $\overline{[u'(z)]^2}$ with the help of the polarization relations for GW.

[25] **Acknowledgments.** This work was supported by German Research Foundation (DFG) grants PA 477/2-1 and HA 3261/2-3.

References

Castle, K. J., K. M. Kleissas, J. M. Rhinehart, E. S. Hwang, and J. A. Dodd (2006), Vibrational relaxation of $CO_2(\nu_2)$ by atomic oxygen, *J. Geophys. Res.*, *111*, A09303, doi:10.1029/2006JA011736.

Fomichev, V. I., A. A. Kutepov, R. A. Akmaev, and G. M. Shved (1993), Parameterization of the 15-micron CO_2 band cooling in the middle atmosphere (15–115 km), *J. Atmos. Terr. Phys.*, *55*, 7–18.

Fritts, D. C., and M. J. Alexander (2003), Gravity wave dynamics and effects in the middle atmosphere, *Rev. Geophys.*, *41*(1), 1003, doi:10.1029/2001RG000106.

Gusev, O. A., and A. A. Kutepov (2003), Non-LTE gas in planetary atmospheres, in *Stellar Atmosphere Modeling*, *ASP Conf. Ser.*, vol. 288, edited by I. Hubeny, D. Mihalas, and K. Werner, pp. 318–330, Astron. Soc. of the Pacific, San Francisco, Calif.

Hartogh, P., A. S. Medvedev, T. Kuroda, R. Saito, G. Villanueva, A. G. Feofilov, A. A. Kutepov, and U. Berger (2005), Description and climatology of a new general circulation model of the Martian atmosphere, *J. Geophys. Res.*, *110*, E11008, doi:10.1029/2005JE002498.

Kaufmann, M., O. A. Gusev, K. U. Grossmann, R. G. Roble, M. E. Hagan, C. Hartsough, and A. A. Kutepov (2002), The vertical and horizontal distribution of CO_2 densities in the upper mesosphere and lower thermosphere as measured by CRISTA, *J. Geophys. Res.*, *107*(D23), 8182, doi:10.1029/2001JD000704.

Kutepov, A. A., and V. I. Fomichev (1993), Application of the second-order escape probability approximation to the solution of the NLTE vibration-rotational band radiative transfer problem, *J. Atmos. Terr. Phys.*, *55*, 1–6.

Kutepov, A. A., O. A. Gusev, and V. P. Ogibalov (1998), Solution of the non-LTE problem for molecular gas in planetary atmospheres: Superiority of accelerated lambda iteration, *J. Quant. Spectrosc. Radiat. Transfer*, *60*, 199–220.

López-Puertas, M., and F. W. Taylor (2001), *Non-LTE Radiative Transfer in the Atmosphere*, World Sci., Singapore.

Manuilova, R. O., et al. (1998), Modeling of non-LTE limb spectra of ir ozone bands for the MIPAS space experiment, *J. Quant. Spectrosc. Radiat. Transfer*, *59*, 405–422.

Medvedev, A. S., and G. P. Klaassen (2000), Parameterization of gravity wave momentum deposition based on nonlinear wave interactions: Basic formulation and sensitivity tests, *J. Atmos. Sol. Terr. Phys.*, *62*, 1015–1033.

Medvedev, A. S., and G. P. Klaassen (2003), Thermal effects of saturating gravity waves in the atmosphere, *J. Geophys. Res.*, *108*(D2), 4040, doi:10.1029/2002JD002504.

Sharma, R. D., and P. P. Wintersteiner (1990), Role of carbon dioxide in cooling planetary thermospheres, *Geophys. Res. Lett.*, *17*, 2201–2204.

Shved, G. M., A. A. Kutepov, and V. P. Ogibalov (1998), Non-local thermodynamic equilibrium in CO_2 in the middle atmosphere. 1. Input data and populations of the v_3 mode manifold states, *J. Atmos. Sol. Terr. Phys.*, *60*, 289–314.

Sica, R. J., and A. T. Russell (1999), How many waves are in the gravity wave spectrum?, *Geophys. Res. Lett.*, *26*(24), 3617–3620, doi:10.1029/1999GL003683.

Vadas, S. L., and D. C. Fritts (2005), Thermospheric responses to gravity waves: Influences of increasing viscosity and thermal diffusivity, *J. Geophys. Res.*, *110*, D15103, doi:10.1029/2004JD005574.

Whiteway, J. A., and A. Carswell (1995), Lidar observations of gravity wave activity in the upper stratosphere over Toronto, *J. Geophys. Res.*, *100*(D7), 14,113–14,124.

Zhu, X. (1989), A parameterization of cooling rate calculation under the non-LTE condition: Multi-level model, *Adv. Atmos. Sci.*, *6*, 403–413.

A. G. Feofilov and A. A. Kutepov, NASA Goddard Space Flight Center, Mail Code 674, Greenbelt, MD 20771, USA. (akutepov@pop600.gsfc.nasa.gov)

P. Hartogh and A. S. Medvedev, Max Planck Institute for Solar System Research, Max-Planck-Strasse 2, Katlenburg-Lindau D-37191, Germany.

A. W. A. Pauldrach, University Observatory Munich, Faculty for Physics, Ludwig Maximilian University, Scheinerstrasse 1, Munich D-81679, Germany.